molecular pharmaceutics

Article

pubs.acs.org/molecularpharmaceutics

Hybrid Peptide Dendrimers for Imaging of Chemokine Receptor 4 (CXCR4) Expression

Joeri Kuil,[†,‡] Tessa Buckle,[†,‡] Joppe Oldenburg,[†] Hushan Yuan,[§] Alexander D. Borowsky,[∥] Lee Josephson,[§] and Fijs W. B. van Leeuwen*[,†,‡]

[†]Division of Diagnostic Oncology, The Netherlands Cancer Institute Antoni van Leeuwenhoek Hospital, 1066 CX Amsterdam, The Netherlands

[‡]Department of Radiology, Leiden University Medical Center, 2300 RC Leiden, The Netherlands

[§]Center for Translational Nuclear Medicine and Molecular Imaging, Massachusetts General Hospital and Harvard Medical School, Building 149, 13th Street, Charlestown, Massachusetts 02129, United States

[∥]Department of Pathology and Laboratory Medicine, Center for Comparative Medicine, School of Medicine, University of California at Davis, Sacramento, California, United States

Supporting Information

ABSTRACT: The chemokine receptor 4 (CXCR4), which is overexpressed in many types of cancer, is an emerging target in the field of molecular imaging and therapeutics. The CXCR4 binding of several peptides, including the cyclic Ac-TZ14011, has already been validated. In this study mono-, di- and tetrameric Ac-TZ14011-containing dendrimers were prepared and functionalized with a multimodal (hybrid) label, consisting of a Cy5.5-like fluorophore and a DTPA chelate. Confocal microscopy revealed that all three dendrimers were membrane bound at 4 °C, consistent with CXCR4 binding *in vitro*. The unlabeled dimer and tetramer had a somewhat lower affinity for CXCR4 than the unlabeled monomer. However, when labeled with the multimodal label the CXCR4 affinity of the dimer and tetramer was considerably higher compared to that of the labeled monomer. On top of that, biodistribution studies revealed that the additional peptides in the dimer and tetramer reduced nonspecific muscle uptake. Thus, multimerization of the cyclic Ac-TZ14011 peptide reduces the negative influence of the multimodal label on the receptor affinity and the biodistribution.

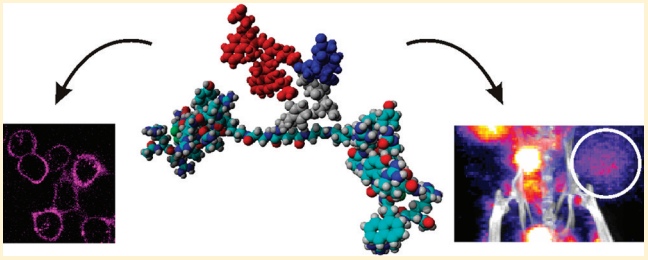

KEYWORDS: *CXCR4, peptides, dendrimers, multimodal hybrid imaging, fluorescence, SPECT/CT*

INTRODUCTION

The chemokine receptor 4 (CXCR4) is a G-protein-coupled membrane receptor that is overexpressed in 23 types of cancer where it plays a role in, among other things, the metastatic spread.[1−3] For this reason it is an emerging biomarker in the field of diagnostic oncology.[4] CXCR4 is also used as a target for cancer therapy and chemosensitization.[5−7] Several peptide antagonists for CXCR4 have been developed,[8,9] including the potent 14 amino acid-containing disulfide-bridged Ac-TZ14011 cyclic peptide (Scheme 1).[10−13] The pharmacophore of this peptide consists of residues 2, 3, 5 and 14, and the peptide has only one free amine (D-Lys[8]), which is distant from the pharmacophore.[12,13] Several fluorescent dyes and indium-labeled DTPA have been used to label Ac-TZ14011 at D-Lys[8], and with these conjugates the CXCR4 binding has been validated *in vitro* and *in vivo*.[10−16] Recently we reported the first hybrid CXCR4 peptide, which consisted of Ac-TZ14011 and a multifunctional single attachment point (MSAP) label.[10] This MSAP label comprised a DTPA chelate and a CyAL-5.5$_b$ fluorophore.[17−19]

The development of multimodal probes is attaining a significant interest in the field of molecular imaging.[20−25] Such probes can be used in more than one imaging modality. Important imaging modalities are radionuclide-based imaging (SPECT and PET) and fluorescence-based optical imaging. Each modality has its own strengths and weaknesses, and therefore, a combination of modalities is often used in the clinic for optimal detection. Recently we have shown the added value of multimodal imaging agents in preclinical surgical guidance[10,26,27] and even in patients.[28] Multimodal probes can in principle also be used for postoperative pathology and assessment for the effectiveness of chemo- and/or immunotherapy.

Several receptor targeting peptides (e.g., RGD, octreotate, bombesin and Ac-TZ14011) have been functionalized with labels that combine radioactivity and fluorescence.[10,20] Such

Received: August 12, 2011
Revised: October 12, 2011
Accepted: October 25, 2011
Published: November 15, 2011

Scheme 1. Synthesis of Dimer $(Ac\text{-}TZ14011)_2$ (6), Dimer $(Ac\text{-}TZ14011)_2$-MSAP (7), Tetramer $(Ac\text{-}TZ14011)_4$ (9) and Tetramer $(Ac\text{-}TZ14011)_4$-MSAP (10) and the Structures of MSAP Reagent (1), Ac-TZ14011 (2) and Monomer Ac-TZ14011-MSAP (3)

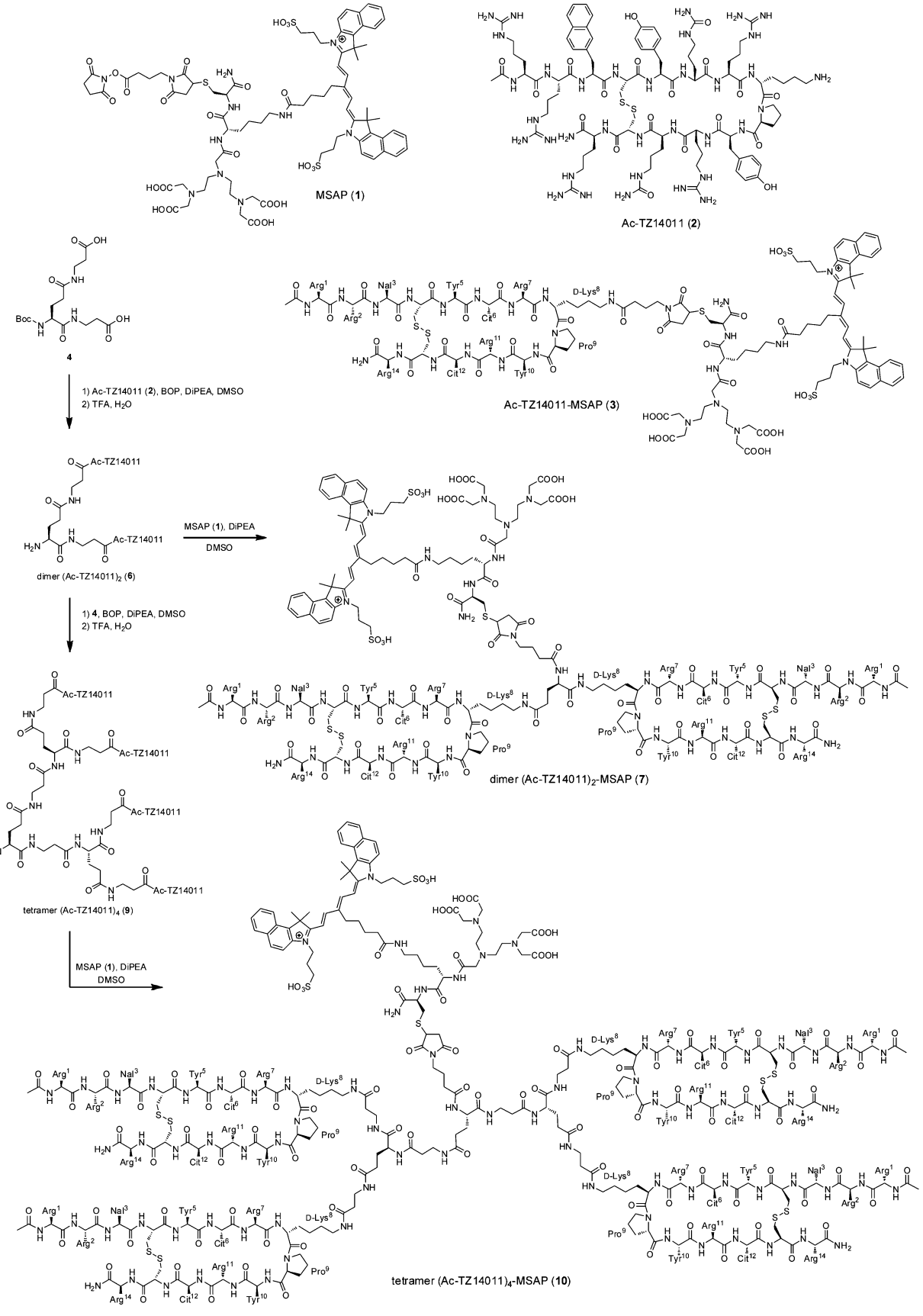

dx.doi.org/10.1021/mp200401p | Mol. Pharmaceutics 2011, 8, 2444–2453

labels are often as large as the peptide used for the (tumor) specificity. Therefore, this hybrid labeling technology can have a significant (negative) influence on the receptor binding and the biodistribution. Especially the dye-driven, nonspecific uptake by organs and tissues is a substantial concern.[20] We reasoned in a recent review that multimeric peptide dendrimers, consisting of multiple peptides (e.g., 4) and one hybrid label, could reduce the influence of the label.[20] Multimerization is well-known to enhance the receptor affinity and specificity.[29−35] On top of that, multimerization increases the amount of peptides with respect to the label, which may help shield the label from the biological environment.[20]

The strategy of peptide multimerization has already been successfully applied with radiolabels and fluorescent labels.[36−40] However, only nanosized multimeric peptides have been prepared with both a radiolabel and a fluorescent label.[41,42] Despite the fact that nanoparticles can in general benefit from the enhanced permeability and retention (EPR) effect,[43] these specific "large" nanoparticles suffered from high nonspecific (liver) uptake and were not able to extravasate from blood vessels into the tumor.[41,42] Surprisingly, small hybrid peptide dendrimers, which generally have a better biodistribution, have never been reported. Here, we report the first hybrid Ac-TZ14011-containing dimeric and tetrameric dendrimers. These dendrimers are based on our previously reported multimodal Ac-TZ14011-MSAP peptide (**3**) (Scheme 1).[10]

EXPERIMENTAL SECTION

Cell Culture. The human breast cancer cell line MDAMB231^{CXCR4+} was kindly provided by Ed Roos (NKI-AvL, Amsterdam, The Netherlands). MDAMB231^{CXCR4+} cells were selected by flow cytometry based on their high CXCR4-expression levels. The cell line was maintained in Gibco's minimum essential medium (MEM) enriched with 10% fetal bovine serum, penicillin/streptomycin, L-glutamine, nonessential amino acids, sodium pyruvate and MEM vitamins solution (all Life Technologies Inc.). Cells were kept under standard culture conditions.

Confocal Microscopy. MDAMB231^{CXCR4+} cells were seeded onto coverslips (⌀ 24 mm; Karl Hecht GmbH & Co.) and incubated overnight. The cells were washed with medium, incubated with 1 μM compound in medium for 1 h at 4 °C and washed again with ice cold phosphate buffered saline (PBS). Confocal microscopy images were taken at 37 °C on a Leica TCS-SP2-AOBS Live confocal microscope (Leica Microsystems Heidelberg GmbH).

Prior to the incubation of the MSAP label (**1**), the active NHS ester was hydrolyzed: 150 μg of MSAP (**1**) was dissolved in 29 μL of EtOH, 262 μL of H_2O and 2.5 μL of 4 M NaOH. After 1 h stirring at 20 °C, 3 μL of AcOH was added to neutralize the solution. This stock solution was further diluted in medium.

Determination of Dissociation Constants by Flow Cytometry. MDAMB231^{CXCR4+} cells were trypsinized and aliquoted in portions of 300000 cells. For saturation binding experiments, different concentrations of **7** or **10** ranging between 0 and 1000 nM in 50 μL of 0.1% bovine serum albumin (BSA) in PBS were added. For competition experiments different concentrations (0−100000 nM) of **6** or **9** in the presence of 250 nM **3** in 50 μL of 0.1% BSA in PBS were added. Cells were incubated for 1 h at 4 °C. The cells were washed (2×) with 300 μL of 0.1% BSA in PBS and resuspended in 300 μL of 0.1% BSA in PBS, and fluorescence was measured using a CyAn ADP flow cytometer (DakoCytomation) with APC-Cy7 settings (635 nm laser and 750 nm long pass filter). Live cells were gated on Forward Scatter, Side Scatter and Pulse Width, and 20000 viable cells were analyzed. All experiments were performed in duplicate.

The normalized geometric means were fitted with equations in the GraphPad Prism 5 software. The K_D values of **7** and **10** were calculated using the "Binding − Saturation, One site − Total" nonlinear regression equation (eq 1). The K_D values of **6** and **9** were calculated using the "Binding − Competitive, One site − Fit K_i" nonlinear regression equation (eqs 2 and 3). The K_D values of **3** (186.9 nM) and **2** (8.61 nM) have previously been reported.[10]

$$y = \frac{B_{max}x}{K_D + x} + \mathrm{NS}\,x + \mathrm{background} \quad (1)$$

where y = normalized fluorescence, B_{max} = maximum specific binding in the units of the y axis, x = concentration of **7** or **10** in nM, K_D = equilibrium dissociation constant of **7** or **10** in nM, NS = slope of nonspecific binding and background = amount of normalized fluorescence with no added compound.

$$\log \mathrm{IC}_{50} = \log\left(10^{\log K_D}\left(1 + \frac{[\mathbf{3}]}{K_{D,\mathbf{3}}}\right)\right) \quad (2)$$

$$y = \mathrm{bottom} + \frac{\mathrm{top} - \mathrm{bottom}}{1 + 10^{(x - \log \mathrm{IC}_{50})}} \quad (3)$$

where IC_{50} = concentration of competitor that results in binding halfway between bottom and top, K_D = equilibrium dissociation constant of the competitor in nM, [**3**] = concentration of **3** (250 nM), $K_{D,3}$ = dissociation constant of **3** (186.9 nM), y = normalized fluorescence and bottom and top = plateaus in the units of the y axis.

Cell Viability Analysis. Cell viability, based on the percentage of gated cells, was assessed using the flow cytometry data obtained from the saturation binding and competition experiments. For compounds **3**, **7** and **10** the percentage of gated cells when no compound was added was defined as 100% and the percentage of gated cells for the different concentrations of **3**, **7** and **10** was calculated with respect to this. For compounds **2**, **6** and **9** the percentage of gated cells when only 250 nM Ac-TZ14011-MSAP (**3**) was added was defined as 100% and the percentage of gated cells for the different concentrations of **2**, **6** and **9** was calculated with respect to this.

***In Vivo* Model.** For generation of the CXCR4-positive mouse tumor lesions, FVB mice (n = 3 for each compound; 3−4 weeks of age) were used. Before MIN-O lesion segment transplantation (and imaging), mice were anesthetized using a hypnorm (VetaPharma Ltd.)/dormicum (Midazolam; Roche)/water solution (1:1:2; 5 μL/g ip). Via a small incision, the inguinal lymph node was excised, whereafter a piece of preinvasive 8w-B MIN-O tissue was placed into the remaining tissue of the fourth mammary gland.[44−46] Approximately 6−8 weeks after transplantation, lesions were deemed suitable for further experiments (0.8−1 cm in diameter). All animal experiments were performed in accordance with Dutch welfare regulations and approved by the local ethics committee.

Radiolabeling. Compounds **3**, **7** and **10** were dissolved in 0.1 M acetic acid (50 μg/100 μL), and $InCl_3$ (10 MBq/50 μg of compound; Covidien-Mallinckrodt) was added. After 30 min of

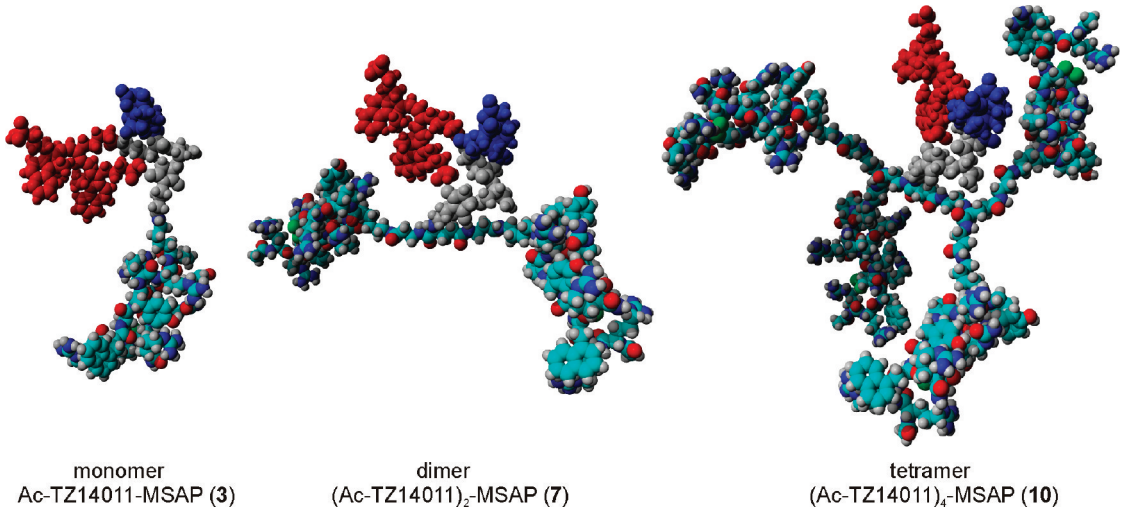

Figure 1. Molecular models of the mono-, di- and tetrameric Ac-TZ14011 dendrimers with the MSAP label. For clarity, the MSAP label is not colored by element: the CyAL-5.5$_b$ fluorophore is displayed in red, the indium-bound DTPA chelate in blue and the spacer in gray. In the dimer and, especially, in the tetramer a smaller percentage of the whole molecule comprises the MSAP label.

incubation, the labeling was validated with TLC using 74 mM of sodium citrate (pH 5) as an eluent and a VCS-201 TLC scanner (Veenstra Instruments). In all cases, labeling efficacy was >99%. Before injection, the solution was diluted (1:1) with saline (0.90% w/v of NaCl in water).

Prior to ^{111}In labeling of MSAP label (**1**), the active NHS ester was hydrolyzed as described for confocal microscopy.

Single Photon Emission Computed Tomography (SPECT)/Computed Tomography (CT). Twenty-four hours after intravenous injection of 50 μg of ^{111}In-labeled compound (10 MBq), the mice were placed in a temperature controlled (37 °C) animal holder (Equipment Veterinaire MINERVE) before a SPECT/CT scan was performed on the nanoSPECT/CT (Bioscan Inc.). The region of interest (ROI) incorporating the whole body was selected based on a (sagital) tomographic planning X-ray image followed by a helical 3D CT. After ROI selection, a sequential total body SPECT scan of the same field of view was performed. After acquisition, the data was reconstructed with HiSPECT software (Scivis GmbH). The SPECT and CT data sets were automatically coregistered. The images were analyzed using the InVivoScope post processing software (Bioscan Inc.).

Biodistribution Studies. After SPECT/CT imaging, tissues were excised. Tissues were weighed, and the amount of radioactivity present in the tissues was counted using a Perkin-Elmer 1480 Wizard 3″ automatic gamma counter (245 keV; 60 s). Counts per minute were converted into MBq and corrected for decay. The percentage of the injected dose per gram of tissue (% ID/g) was calculated as follows: [(MBq measured in tissue/injected dose) × 100%]/weight of tissue. *P* values were calculated using an unpaired *t* test (GraphPad).

RESULTS AND DISCUSSION

Design and Synthesis. The main aim of our chemical design was to minimize the negative influence of the multimodal MSAP label on receptor binding and tumor targeting observed for the previously reported monomer Ac-TZ14011-MSAP (**3**).[10] To achieve this, we prepared dimeric and tetrameric dendrimers, where the MSAP label is placed in the core of the dendrimer (Figure 1). The dendrimers were based on glutamic acid. Additional β-alanine spacers were incorporated to ensure that the peptide epitopes would not hinder the CXCR4 binding of the other peptides. The design of the compounds was verified by inserting the respective models of Figure 1 into the crystal structure of CXCR4 using the modeling program Yasara.[47] The modeling data suggested that the spacers are long enough to avoid steric hindrance (see Figure S1 in the Supporting Information). The relatively short spacers that were used enable the shielding of the MSAP label from the biological environment by the peptides (Figure 1). As a consequence of the short spacers, the different peptide moieties on the dendrimers will most likely not be able the bind multiple CXCR4 receptors simultaneously. It has been reported that larger spacers of 5.5−6.5 nm are required to achieve this.[48] However, our design can increase the binding affinity via an effect named statistical rebinding.[29−31] Statistical rebinding is caused by an overall slower off-rate of the multimeric compound due to the close proximity of other CXCR4-binding peptide epitopes, which can replace the bound peptide when released from the binding site.

The synthesis of the dendrimers is outlined in Scheme 1 and is described in detail in the Supporting Information. First Boc-Glu(β-Ala-OH)-β-Ala-OH (**4**) was prepared, after which it was functionalized with Ac-TZ14011 (**2**), resulting in the Boc-protected dimer (Ac-TZ14011)$_2$ (**5**) in 58% yield after HPLC purification (Scheme 1). The Boc group was removed with TFA, and the MSAP reagent (**1**) was attached to the free amine in the core of the derivative **6**, yielding multimodal compound **7** as a blue fluffy solid in a satisfactory 69% yield. Alternatively, an excess of dimeric derivative **5** was reacted with Boc-Glu(β-Ala-OH)-β-Ala-OH (**4**) to obtain the Boc-protected tetrameric peptide dendrimer **8**. Boc deprotection and subsequently conjugation with compound **1** yielded the tetrameric MSAP derivative **10** in 50%, which suggests that the peptides did not substantially hinder the coupling reaction.

***In Vitro* Evaluation.** Previously we have demonstrated that monomer Ac-TZ14011-MSAP (**3**) was able to discriminate between MDAMB231 cells, which express basal levels of CXCR4, and MDAMB231^{CXCR4+} cells, which overexpress CXCR4 4-fold.[10] Furthermore, the binding affinity of Ac-TZ14011 (**2**) and Ac-TZ14011-MSAP (**3**) for CXCR4 has been established.[10] *In vitro* studies regarding the binding affinity

dx.doi.org/10.1021/mp200401p | *Mol. Pharmaceutics* 2011, 8, 2444−2453

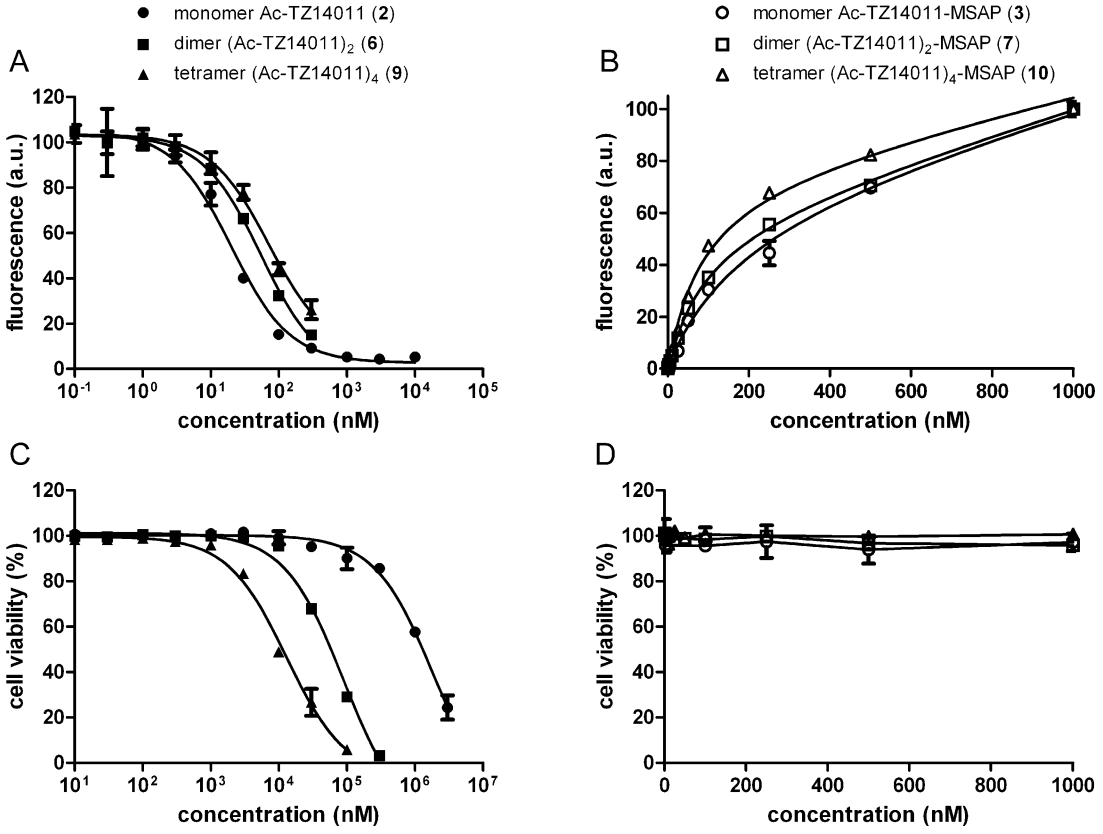

Figure 2. (A) Competition experiments of the compounds **2**, **6** and **9** in the presence of 250 nM of Ac-TZ14011-MSAP (**3**). (B) Saturation binding experiments of compounds **3**, **7** and **10**. (C, D) Cell viability of MDAMB231^{CXCR4+} cells in the presence of different concentrations compounds **2**, **6** and **9** (C) and compounds **3**, **7** and **10** (D). For all graphs the bars represent average ± SD.

are the most reliable point of comparison for the Ac-TZ14011-based dendrimers.

The CXCR4 receptor affinity of the unlabeled constructs was determined using a previously reported cell-based competition assay, where the unlabeled peptides compete with monomer Ac-TZ14011-MSAP (**3**) for binding to MDAMB231^{CXCR4+} cells (Figure 2A).[10] The dissociation constant (K_D) of the monomer Ac-TZ14011 (**2**) has previously been reported to be 8.61 nM (Table 1).[10] The receptor affinity of both dimer (Ac-TZ14011)$_2$ (**6**) and tetramer (Ac-TZ14011)$_4$ (**9**) was found to be somewhat lower: 23.5 nM and 30.6 nM, respectively. A multivalency effect based on e.g. bivalent binding or statistical rebinding was not observed, but rather a slight decrease in affinity. We previously reported iridium complexes outfitted with one, two or three Ac-TZ14011 peptides that also did not display a considerable multivalency effect.[11] Moreover, Tanaka et al. have shown that bivalent pentapeptidic CXCR4 ligands with spacers larger than 4.5 nm (15 proline residues) only display a modest increase in affinity of maximal 3.2-fold due to multivalent interactions.[48] These findings are not uncommon for peptides binding to G-protein coupled receptors (GPCRs), as multimeric octreotides also do not bind in a multivalent manner to the somatostatin GPCR.[49,50] It is apparently very challenging to design relatively small dendrimers that can position peptide-binding epitopes correctly for simultaneous binding to multiple GPCRs.

Table 1. Dissociation Constants (K_D) of the Ac-TZ14011 Derivatives

	unlabeled derivs		MSAP-labeled derivs	
	compd	K_D (nM)	compd	K_D (nM)
monomers	**2**	8.61 ± 1.42	**3**	186.9 ± 52.4
dimers	**6**	23.5 ± 2.43	**7**	93.1 ± 10.1
tetramers	**9**	30.6 ± 4.84	**10**	80.5 ± 11.6

The receptor affinity of the MSAP-labeled constructs **3**, **7** and **10** was determined using saturation binding experiments (Figure 2B). The affinity of the monomer Ac-TZ14011-MSAP (**3**) amounts to 186.9 nM (Table 1).[10] Interestingly, the dimer (Ac-TZ14011)$_2$-MSAP (**7**) had a 2-fold higher affinity, namely, 93.1 nM. This clear effect is in contrast with the trend found for the unlabeled peptide derivatives; the unlabeled dimer (Ac-TZ14011)$_2$ (**6**) had an almost 3-fold decrease in affinity compared to the monomer Ac-TZ14011 (**2**) (Table 1). It seems that the additional peptide moiety reduces the negative influence the MSAP label has on the receptor affinity. For the tetramer (Ac-TZ14011)$_4$-MSAP (**10**) a similar effect was observed (K_D = 80.5 nM), although the improvement with respect to dimer (Ac-TZ14011)$_2$-MSAP (**7**) was minimal. However, the saturation binding curve showed that the nonspecific cell binding was considerably reduced for the tetramer (Ac-TZ14011)$_4$-MSAP (**10**), i.e. the linear part of the curve is less steep than that of the monomer Ac-TZ14011-MSAP (**3**) (Figure 2B and eq 1). This suggests that the peptides in tetramer **10** indeed shield the MSAP label from nonspecific cell membrane binding, as was designed.

Next to the CXCR4 affinity studies with flow cytometry, the cellular distribution of the MSAP-labeled compounds **3**, **7** and **10** was evaluated using confocal microscopy.

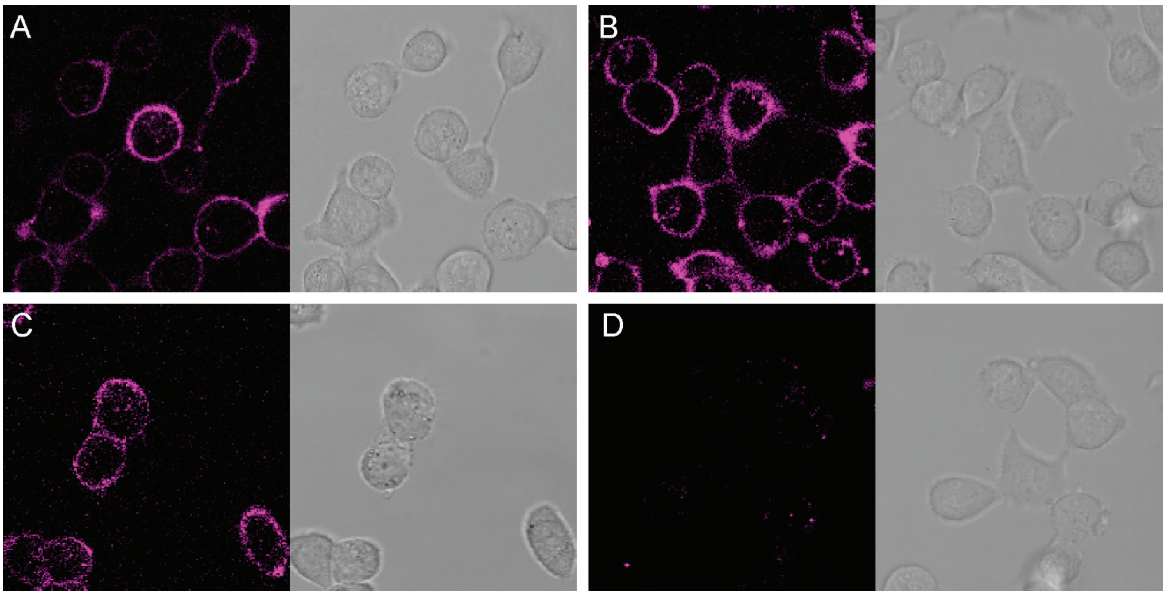

Figure 3. Confocal microscopy and transmission images of the multimodal peptide conjugates on MDAMB231^{CXCR4+} cells: (A) 1 μM monomer Ac-TZ14011-MSAP (**3**); (B) 1 μM dimer (Ac-TZ14011)$_2$-MSAP (**6**); (C) 1 μM tetramer (Ac-TZ14011)$_4$-MSAP (**10**); (D) 1 μM MSAP label (**1**).

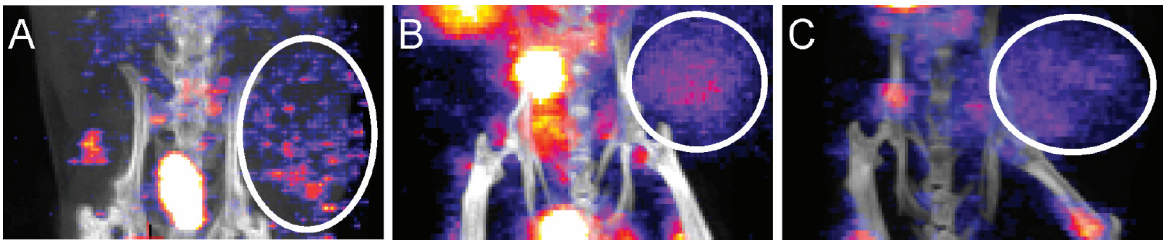

Figure 4. SPECT/CT of (A) monomer Ac-TZ14011-MSAP (**3**), (B) dimer (Ac-TZ14011)$_2$-MSAP (**7**) and (C) tetramer (Ac-TZ14011)$_4$-MSAP (**10**).

MDAMB231^{CXCR4+} cells were incubated with 1 μM compound for 1 h at 4 °C, to minimize active internalization. All three peptide conjugates (**3**, **7** and **10**) displayed cell membrane staining (Figure 3), which is in accordance with the location of the CXCR4 receptor.[10−13] Also a small amount of internalization of compounds **3**, **7** and **10** was observed. This internalization was most likely caused by the fact that the confocal imaging was performed at 37 °C, resulting in some receptor mediated endocytosis during the image acquisition. As a negative control, cells were incubated with the MSAP label (**1**) alone, of which the active NHS ester was hydrolyzed prior incubation. The MSAP label alone showed almost no staining (Figure 3D), and therefore, the cell membrane staining pattern of compounds **3**, **7** and **10** is driven by the targeting peptide moieties and is not caused by nonspecific cell membrane binding of the MSAP label.

The effect of the monomers **2** and **3**, dimers **6** and **7** and tetramers **9** and **10** on the cell viability during the K_D determination was measured to exclude any artifacts (Figure 2C,D); reduced cell viability may increase nonspecific binding and/or uptake. These data show that none of the six compounds had an influence on the cell viability up to concentrations of 1 μM. At higher concentrations first the tetramer (Ac-TZ14011)$_4$ (**9**) displayed toxic effects (IC_{50} = 13.0 μM ± 0.29), then the dimer (Ac-TZ14011)$_2$ (**6**) (IC_{50} = 88.9 μM ± 8.77), and last the monomer Ac-TZ14011 (**2**) (IC_{50} = 1912 μM ± 285) (Figure 2C). The trend that the increasing multimeric character of the Ac-TZ14011 peptide leads to more cytotoxicity has previously been observed by us and is most likely a charge-related effect.[11] The monomeric construct **2** is +6 charged, the dimeric construct **6** is +11 charged and the tetrameric construct **9** is +21 charged. We reason that this increase in positive charge may result in charge-driven (nonspecific) membrane binding and cause cytotoxicity, similar to that reported for positively charged PAMAM dendrimers.[11,51]

Based on the *in vitro* experiments the dimer (Ac-TZ14011)$_2$-MSAP (**7**) seems to be the most promising imaging candidate. It has practically the same high affinity for CXCR4 as the tetramer (Ac-TZ14011)$_4$-MSAP (**10**), has considerable less influence on the cell viability and is easier to prepare than the tetravalent derivative **10**.

***In Vivo* Evaluation.** *In vivo* imaging studies were performed to evaluate the tumor targeting of the MSAP peptides **3**, **7** and **10**. Similar to previous studies,[10] mice with CXCR4 positive "spontaneous" MIN-O lesions[44−46] (0.8−1 cm in diameter) were used instead of the MDAMB231^{CXCR4+} cell line. The CXCR4 expression in MDAMB231^{CXCR4+} cells decreases to basal levels *in vivo*, whereas we have reported that the MIN-O lesions express CXCR4 *in vivo*.[10,52] Because the MIN-O tumor model is based on tissue transplantation, it can only be maintained in mice and until now efforts to derive cell lines for *in vitro* studies have not been successful. This thus

dx.doi.org/10.1021/mp200401p | *Mol. Pharmaceutics* 2011, 8, 2444−2453

Table 2. Biodistribution of ^{111}In-Labeled Ac-TZ14011-DTPA (11), MSAP Label (1), Monomer Ac-TZ14011-MSAP (3), Dimer $(Ac\text{-}TZ14011)_2$-MSAP (7) and Tetramer $(Ac\text{-}TZ14011)_4$-MSAP (10) in MIN-O Tumor Bearing Mice at 24 h Postinjection

	uptake[a] (% ID/g)				
tissue	**11**	**1**	**3**	**7**	**10**
blood	0.01 ± 0.00	0.32 ± 0.09**	0.14 ± 0.02***	0.14 ± 0.03**	0.11 ± 0.01***
brain	0.00 ± 0.00	0.03 ± 0.01	0.02 ± 0.00	0.03 ± 0.01	0.02 ± 0.00
lungs	0.13 ± 0.02	0.65 ± 0.18**	1.02 ± 0.13***	2.13 ± 0.60**	1.68 ± 0.31**
heart	0.05 ± 0.00	0.64 ± 0.12**	0.89 ± 0.22**	0.60 ± 0.12**	0.43 ± 0.06***
liver	5.08 ± 0.52	5.76 ± 1.11	22.46 ± 5.46**	30.59 ± 5.45**	22.43 ± 0.67***
kidneys	27.07 ± 0.74	6.49 ± 2.99***	7.50 ± 1.39***	6.46 ± 1.36***	4.37 ± 0.52***
spleen	1.14 ± 0.32	0.93 ± 0.13	4.76 ± 1.23**	7.01 ± 1.45**	4.66 ± 0.46***
stomach	0.06 ± 0.01	0.81 ± 0.45*	0.81 ± 0.16**	0.97 ± 0.52*	1.09 ± 0.52*
intestines	0.10 ± 0.01	1.02 ± 0.31**	1.85 ± 0.08***	2.06 ± 0.26***	1.56 ± 0.46**
tumor	0.19 ± 0.03	n.d.	1.10 ± 0.60	0.57 ± 0.19*	0.42 ± 0.10*
muscle (paw)	0.03 ± 0.00	0.22 ± 0.06**	0.31 ± 0.01***	0.07 ± 0.03	0.08 ± 0.02*

[a]The significance with respect to ^{111}In-labeled Ac-TZ14011-DTPA (**11**) is indicated by the asterisks (*P < 0.05, **P < 0.01, ***P < 0.001).

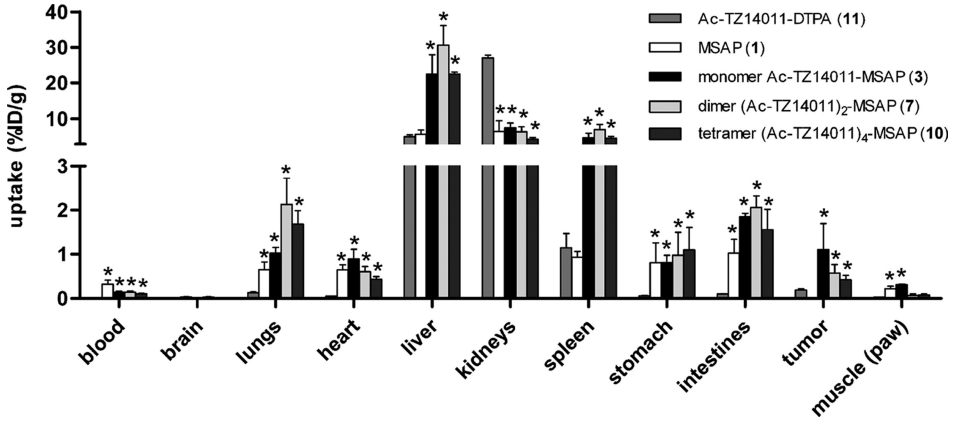

Figure 5. Biodistribution of ^{111}In-labeled Ac-TZ14011-DTPA (**11**), MSAP label (**1**), monomer Ac-TZ14011-MSAP (**3**), dimer $(Ac\text{-}TZ14011)_2$-MSAP (**7**) and tetramer $(Ac\text{-}TZ14011)_4$-MSAP (**10**) in MIN-O tumor bearing mice at 24 h postinjection. Significant differences (P < 0.05) with respect to ^{111}In-labeled Ac-TZ14011-DTPA (**11**) are indicated by the asterisks (see Table 2 for distinction between P < 0.05, P < 0.01 and P < 0.001).

dictates the use of both the $MDAMB231^{CXCR4+}$ cells and the MIN-O tumor model.

Mice were injected with ^{111}In-labeled compounds **3**, **7** and **10**, and after 24 h the mice were imaged with SPECT/CT imaging (Figure 4). With all three compounds (**3**, **7** and **10**) the tumors could be visualized. However, based on the SPECT/CT images it is not possible to deduce the percentages injected dose per gram (% ID/g). The latter requires *ex vivo* analysis, and therefore, after imaging, the mice were sacrificed and biodistribution studies were conducted (Table 2 and Figure 5). As a reference also the biodistribution of the previously reported peptide with only a DTPA chelate as an imaging label, Ac-TZ14011-DTPA (**11**), is given (see Supporting Information for the structure).[16] As a negative control, the MSAP label (**1**) was used without further functionalization (reactive group was neutralized) in non-tumor bearing mice.

The MSAP label (**1**) alone only had a reduced kidney uptake compared to Ac-TZ14011-DTPA (**11**) (Table 2 and Figure 5). The monomer Ac-TZ14011-MSAP (**3**) gave increased liver and intestinal uptake and reduced kidney uptake compared to the reference Ac-TZ14011-DTPA (**11**), suggesting a change in the clearance route (Table 2 and Figure 5). The monomer Ac-TZ14011-MSAP (**3**) displayed a more than five times higher tumor uptake than Ac-TZ14011-DTPA (**11**). However, this increase was accompanied with higher nonspecific uptake in the lungs, heart, spleen, stomach, intestines and muscles, most likely caused by nonspecific binding of the relative hydrophobic CyAL-5.5_b fluorophore. This resulted in a lower tumor-to-muscle ratio compared to Ac-TZ14011-DTPA (**11**), 4.55 and 6.67, respectively (Table 3). As mentioned in the Introduction,

Table 3. Tumor-to-Muscle Ratios Derived from the Biodistribution Studies

compd	tumor-to-muscle ratio	rel ratio compared to **11**
11	6.67 ± 0.66	1
3	4.55 ± 0.68* [a]	0.68
7	7.41 ± 1.87	1.11
10	5.47 ± 0.50	0.82

[a]P < 0.05 for the comparison of compound **3** with **11**.

an increase in nonspecific binding and a reduction in tumor-to-muscle ratio is a common effect when monomeric multimodal peptides are generated.[20] The most likely reason for this is the relatively large size of the hybrid imaging label.

The dimer $(Ac\text{-}TZ14011)_2$-MSAP (**7**) had a similar uptake profile as monomer Ac-TZ14011-MSAP (**3**) (Table 2 and Figure 5). However, the muscle uptake was significantly lower than that of the monomeric MSAP peptide (P < 0.001; all significant differences with respect to compound **3** are denoted

in Table S1 in the Supporting Information). Thus, the enhanced nonspecific muscle uptake of monomer Ac-TZ14011-MSAP (**3**) compared to Ac-TZ14011-DTPA (**11**) is largely eliminated by the additional peptide moiety in compound **7**. Also the tumor and heart uptake was lower than that of monomer Ac-TZ14011-MSAP (**3**), although this difference was not significant. The decrease of the uptake in the muscle and heart was larger than in the tumor, resulting in an improved tumor-to-muscle ratio of 7.41 (Table 3). This improvement again was not significant, because the standard deviation found for dimer $(Ac\text{-}TZ14011)_2$-MSAP (**7**) was rather high (see Table 3).

The tetramer $(Ac\text{-}TZ14011)_4$-MSAP (**10**) continued the trend of the monomer and dimer (Table 2 and Figure 5). The uptake in the tumor and in the heart was slightly lower than that of dimer $(Ac\text{-}TZ14011)_2$-MSAP (**7**), while uptake in muscle was not reduced further for the tetramer $(Ac\text{-}TZ14011)_4$-MSAP (**10**). As a consequence, the tumor-to-muscle ratio of the tetramer was lower than that of the dimer (**7**) (5.47 and 7.41, respectively; Table 3). Nonspecific uptake of tetramer $(Ac\text{-}TZ14011)_4$-MSAP (**10**) in organs such as the lungs, heart and liver was also slightly lower compared to the dimer $(Ac\text{-}TZ14011)_2$-MSAP (**7**). Thus, the two additional peptides seem to have decreased the MSAP label driven nonspecific uptake even further, resulting in a slightly lower nonspecific retention of tetramer $(Ac\text{-}TZ14011)_4$-MSAP (**10**) in the organs and the tumor, and therefore, an overall somewhat faster clearance from the body. Faster clearance is generally accompanied with reduced blood concentrations and, therefore, reduced amounts of compound available for receptor binding in the tumor. This effect apparently canceled out the higher CXCR4 affinity of tetramer $(Ac\text{-}TZ14011)_4$-MSAP (**10**) compared to dimer $(Ac\text{-}TZ14011)_2$-MSAP (**7**), resulting in a slightly reduced tumor uptake.

The results of the *in vivo* studies show that the additional peptide in dimer **7** reduced the negative influence of the multimodal MSAP label in monomer **3**, yielding a tumor-to-muscle ratio higher than that of monomer **3** and even than that of Ac-TZ14011-DTPA (**11**). The addition of two more peptides, as in tetramer $(Ac\text{-}TZ14011)_4$-MSAP (**10**), however, did not result in a further improvement of the tumor-to-muscle ratio.

CONCLUSIONS

Multimerization resulted in reduction of the nonspecific binding caused by the multimodal label. The CXCR4 affinity of dimer $(Ac\text{-}TZ14011)_2$-MSAP (**7**) and tetramer $(Ac\text{-}TZ14011)_4$-MSAP (**10**) is comparable. The dimer, however, has less influence on the cell viability, and the tumor-to-muscle ratio of the dimer is higher. Thus, dimer $(Ac\text{-}TZ14011)_2$-MSAP (**7**) is the most promising CXCR4 imaging probe.

This concept of multimerization of multimodal peptides can also be applied to other targeting peptides such as RGD. It seems that the use of highly positively charged peptides and highly hydrophobic peptides should be avoided to suppress the cytotoxicity and the nonspecific cell and tissue binding. In this manner our concept could result in even more promising imaging agents.

ASSOCIATED CONTENT

Supporting Information

Molecular modeling protocols, synthetic procedures and statistical analysis of the biodistribution data with respect to compound **3**. This material is available free of charge via the Internet at http://pubs.acs.org.

AUTHOR INFORMATION

Corresponding Author

*Leiden University Medical Center, Radiology, Albinusdreef 2, 2300 RC Leiden, The Netherlands. E-mail: f.w.b.van_leeuwen@lumc.nl. Phone: +31(0)71 526 3491. Fax: 31(0)71 5248256.

ACKNOWLEDGMENTS

This research is supported, in part, by a KWF-translational research award (Grant No. PGF 2009-4344; F.W.B.v.L.), and within the framework of CTMM, the Centre for Translational Molecular Medicine (http://www.ctmm.nl), project Breast CARE (Grant 030-104; J.K.).

REFERENCES

(1) Teicher, B. A.; Fricker, S. P. CXCL12 (SDF-1)/CXCR4 pathway in cancer. *Clin. Cancer Res.* **2010**, *16*, 2927−2931.

(2) Kulbe, H.; Levinson, N. R.; Balkwill, F.; Wilson, J. L. The chemokine network in cancer−much more than directing cell movement. *Int. J. Dev. Biol.* **2004**, *48*, 489−496.

(3) Furusato, B.; Mohamed, A.; Uhlen, M.; Rhim, J. S. CXCR4 and cancer. *Pathol. Int.* **2010**, *60*, 497−505.

(4) Nimmagadda, S.; Pullambhatla, M.; Stone, K.; Green, G.; Bhujwalla, Z. M.; Pomper, M. G. Molecular imaging of CXCR4 receptor expression in human cancer xenografts with [^{64}Cu]AMD3100 positron emission tomography. *Cancer Res.* **2010**, *70*, 3935−3944.

(5) Hassan, S.; Buchanan, M.; Jahan, K.; Aguilar-Mahecha, A.; Gaboury, L.; Muller, W. J.; Alsawafi, Y.; Mourskaia, A. A.; Siegel, P. M.; Salvucci, O.; Basik, M. CXCR4 peptide antagonist inhibits primary breast tumor growth, metastasis and enhances the efficacy of anti-VEGF treatment or docetaxel in a transgenic mouse model. *Int. J. Cancer* **2011**, *129*, 225−232.

(6) Azab, A. K.; Runnels, J. M.; Pitsillides, C.; Moreau, A. S.; Azab, F.; Leleu, X.; Jia, X.; Wright, R.; Ospina, B.; Carlson, A. L.; Alt, C.; Burwick, N.; Roccaro, A. M.; Ngo, H. T.; Farag, M.; Melhem, M. R.; Sacco, A.; Munshi, N. C.; Hideshima, T.; Rollins, B. J.; Anderson, K. C.; Kung, A. L.; Lin, C. P.; Ghobrial, I. M. CXCR4 inhibitor AMD3100 disrupts the interaction of multiple myeloma cells with the bone marrow microenvironment and enhances their sensitivity to therapy. *Blood* **2009**, *113*, 4341−4351.

(7) Nervi, B.; Ramirez, P.; Rettig, M. P.; Uy, G. L.; Holt, M. S.; Ritchey, J. K.; Prior, J. L.; Piwnica-Worms, D.; Bridger, G.; Ley, T. J.; DiPersio, J. F. Chemosensitization of acute myeloid leukemia (AML) following mobilization by the CXCR4 antagonist AMD3100. *Blood* **2009**, *113*, 6206−6214.

(8) Fujii, N.; Oishi, S.; Hiramatsu, K.; Araki, T.; Ueda, S.; Tamamura, H.; Otaka, A.; Kusano, S.; Terakubo, S.; Nakashima, H.; Broach, J. A.; Trent, J. O.; Wang, Z. X.; Peiper, S. C. Molecular-size reduction of a potent CXCR4-chemokine antagonist using orthogonal combination of conformation- and sequence-based libraries. *Angew. Chem., Int. Ed.* **2003**, *42*, 3251−3253.

(9) Tamamura, H.; Hiramatsu, K.; Kusano, S.; Terakubo, S.; Yamamoto, N.; Trent, J. O.; Wang, Z.; Peiper, S. C.; Nakashima, H.; Otaka, A.; Fujii, N. Synthesis of potent CXCR4 inhibitors possessing low cytotoxicity and improved biostability based on T140 derivatives. *Org. Biomol. Chem.* **2003**, *1*, 3656−3662.

(10) Kuil, J.; Buckle, T.; Yuan, H.; Van den Berg, N. S.; Oishi, S.; Fujii, N.; Josephson, L.; Van Leeuwen, F. W. B. Synthesis and evaluation of a bimodal CXCR4 antagonistic peptide. *Bioconjugate Chem.* **2011**, *22*, 859−864.

(11) Kuil, J.; Steunenberg, P.; Chin, P. T. K.; Oldenburg, J.; Jalink, K.; Velders, A. H.; Van Leeuwen, F. W. B. Peptide-functionalized luminescent iridium complexes for lifetime imaging of CXCR4 expression. *ChemBioChem* **2011**, *12*, 1897−1903.

(12) Nomura, W.; Tanabe, Y.; Tsutsumi, H.; Tanaka, T.; Ohba, K.; Yamamoto, N.; Tamamura, H. Fluorophore labeling enables imaging and evaluation of specific CXCR4-ligand interaction at the cell membrane for fluorescence-based screening. *Bioconjugate Chem.* **2008**, *19*, 1917−1920.
(13) Oishi, S.; Masuda, R.; Evans, B.; Ueda, S.; Goto, Y.; Ohno, H.; Hirasawa, A.; Tsujimoto, G.; Wang, Z.; Peiper, S. C.; Naito, T.; Kodama, E.; Matsuoka, M.; Fujii, N. Synthesis and application of fluorescein- and biotin-labeled molecular probes for the chemokine receptor CXCR4. *ChemBioChem* **2008**, *9*, 1154−1158.
(14) Nishizawa, K.; Nishiyama, H.; Oishi, S.; Tanahara, N.; Kotani, H.; Mikami, Y.; Toda, Y.; Evans, B. J.; Peiper, S. C.; Saito, R.; Watanabe, J.; Fujii, N.; Ogawa, O. Fluorescent imaging of high-grade bladder cancer using a specific antagonist for chemokine receptor CXCR4. *Int. J. Cancer* **2010**, *127*, 1180−1187.
(15) Van den Berg, N. S.; Buckle, T.; Kuil, J.; Wesseling, J.; Van Leeuwen, F. W. B. Direct fluorescent detection of CXCR4 using a targeted peptide antagonist. *Transl. Oncol.* **2011**, *4*, 224−230.
(16) Hanaoka, H.; Mukai, T.; Tamamura, H.; Mori, T.; Ishino, S.; Ogawa, K.; Iida, Y.; Doi, R.; Fujii, N.; Saji, H. Development of a ^{111}In-labeled peptide derivative targeting a chemokine receptor, CXCR4, for imaging tumors. *Nucl. Med. Biol.* **2006**, *33*, 489−494.
(17) Shao, F.; Yuan, H.; Josephson, L.; Weissleder, R.; Hilderbrand, S. A. Facile synthesis of monofunctional pentamethine carbocyanine fluorophores. *Dyes Pigments* **2011**, *90*, 119−122.
(18) Garanger, E.; Aikawa, E.; Reynolds, F.; Weissleder, R.; Josephson, L. Simplified syntheses of complex multifunctional nanomaterials. *Chem. Commun.* **2008**, 4792−4794.
(19) Garanger, E.; Blois, J.; Hilderbrand, S. A.; Shao, F.; Josephson, L. Divergent oriented synthesis for the design of reagents for protein conjugation. *J. Comb. Chem.* **2010**, *12*, 57−64.
(20) Kuil, J.; Velders, A. H.; Van Leeuwen, F. W. B. Multimodal tumor-targeting peptides functionalized with both a radio-and a fluorescent-label. *Bioconjugate Chem.* **2010**, *21*, 1709−1719.
(21) Louie, A. Multimodality imaging probes: design and challenges. *Chem. Rev.* **2010**, *110*, 3146−3195.
(22) Thorp-Greenwood, F. L.; Coogan, M. P. Multimodal radio-(PET/SPECT) and fluorescence imaging agents based on metallo-radioisotopes: current applications and prospects for development of new agents. *Dalton Trans.* **2011**, *40*, 6129−6143.
(23) Culver, J.; Akers, W.; Achilefu, S. Multimodality molecular imaging with combined optical and SPECT/PET modalities. *J. Nucl. Med.* **2008**, *49*, 169−172.
(24) Lee, S.; Chen, X. Dual-modality probes for in vivo molecular imaging. *Mol. Imaging* **2009**, *8*, 87−100.
(25) Buckle, T.; Chin, P. T. K.; van Leeuwen, F. W. B. (Non-targeted) radioactive/fluorescent nanoparticles and their potential in combined pre- and intraoperative imaging during sentinel lymph node resection. *Nanotechnology* **2010**, *21*, 482001.
(26) Buckle, T.; van Leeuwen, A. C.; Chin, P. T. K.; Janssen, H.; Muller, S. H.; Jonkers, J.; van Leeuwen, F. W. B. A self-assembled multimodal complex for combined pre- and intraoperative imaging of the sentinel lymph node. *Nanotechnology* **2010**, *21*, 355101.
(27) Buckle, T.; Chin, P. T. K.; van den Berg, N. S.; Loo, C. E.; Koops, W.; Gilhuijs, K. G.; van Leeuwen, F. W. B. Tumor bracketing and safety margin estimation using multimodal marker seeds: a proof of concept. *J. Biomed. Opt.* **2010**, *15*, 056021.
(28) Van der Poel, H. G.; Buckle, T.; Brouwer, O. R.; Valdés Olmos, R. A.; Van Leeuwen, F. W. B. Intraoperative laparoscopic fluorescence guidance to the sentinel lymph node in prostate cancer patients: clinical proof of concept of an integrated functional imaging approach using a multimodal tracer. *Eur. Urol.* **2011**, *60* (4), 826−833.
(29) Kiessling, L. L.; Gestwicki, J. E.; Strong, L. E. Synthetic multivalent ligands as probes of signal transduction. *Angew. Chem., Int. Ed.* **2006**, *45*, 2348−2368.
(30) Pieters, R. J. Maximising multivalency effects in protein-carbohydrate interactions. *Org. Biomol. Chem.* **2009**, *7*, 2013−2025.
(31) Kuil, J.; Branderhorst, H. M.; Pieters, R. J.; de Mol, N. J.; Liskamp, R. M. J. ITAM-derived phosphopeptide-containing dendrimers as multivalent ligands for Syk tandem SH2 domain. *Org. Biomol. Chem.* **2009**, *7*, 4088−4094.
(32) Mammen, M.; Choi, S. K.; Whitesides, G. M. Polyvalent interactions in biological systems: implications for design and use of multivalent ligands and inhibitors. *Angew. Chem., Int. Ed.* **1998**, *37*, 2754−2794.
(33) Lundquist, J. J.; Toone, E. J. The cluster glycoside effect. *Chem. Rev.* **2002**, *102*, 555−578.
(34) Kitov, P. I.; Bundle, D. R. On the nature of the multivalency effect: a thermodynamic model. *J. Am. Chem. Soc.* **2003**, *125*, 16271−16284.
(35) Reczek, J. J.; Kennedy, A. A.; Halbert, B. T.; Urbach, A. R. Multivalent recognition of peptides by modular self-assembled receptors. *J. Am. Chem. Soc.* **2009**, *131*, 2408−2415.
(36) Cheng, Z.; Wu, Y.; Xiong, Z.; Gambhir, S. S.; Chen, X. Near-infrared fluorescent RGD peptides for optical imaging of integrin $\alpha_v\beta_3$ expression in living mice. *Bioconjugate Chem.* **2005**, *16*, 1433−1441.
(37) Liu, S. Radiolabeled cyclic RGD peptides as integrin $\alpha_v\beta_3$-targeted radiotracers: maximizing binding affinity via bivalency. *Bioconjugate Chem.* **2009**, *20*, 2199−2213.
(38) Almutairi, A.; Rossin, R.; Shokeen, M.; Hagooly, A.; Ananth, A.; Capoccia, B.; Guillaudeu, S.; Abendschein, D.; Anderson, C. J.; Welch, M. J.; Frechet, J. M. Biodegradable dendritic positron-emitting nanoprobes for the noninvasive imaging of angiogenesis. *Proc. Natl. Acad. Sci. U.S.A.* **2009**, *106*, 685−690.
(39) Galibert, M.; Sancey, L.; Renaudet, O.; Coll, J. L.; Dumy, P.; Boturyn, D. Application of click-click chemistry to the synthesis of new multivalent RGD conjugates. *Org. Biomol. Chem.* **2010**, *8*, 5133−5138.
(40) Abiraj, K.; Jaccard, H.; Kretzschmar, M.; Helm, L.; Maecke, H. R. Novel DOTA-based prochelator for divalent peptide vectorization: synthesis of dimeric bombesin analogues for multimodality tumor imaging and therapy. *Chem. Commun.* **2008**, 3248−3250.
(41) Cai, W.; Chen, K.; Li, Z. B.; Gambhir, S. S.; Chen, X. Dual-function probe for PET and near-infrared fluorescence imaging of tumor vasculature. *J. Nucl. Med.* **2007**, *48*, 1862−1870.
(42) Boswell, C. A.; Eck, P. K.; Regino, C. A.; Bernardo, M.; Wong, K. J.; Milenic, D. E.; Choyke, P. L.; Brechbiel, M. W. Synthesis, characterization, and biological evaluation of integrin alphavbeta3-targeted PAMAM dendrimers. *Mol. Pharmaceutics* **2008**, *5*, 527−539.
(43) Iyer, A. K.; Khaled, G.; Fang, J.; Maeda, H. Exploiting the enhanced permeability and retention effect for tumor targeting. *Drug Discovery Today* **2006**, *11*, 812−818.
(44) Maglione, J. E.; McGoldrick, E. T.; Young, L. J.; Namba, R.; Gregg, J. P.; Liu, L.; Moghanaki, D.; Ellies, L. G.; Borowsky, A. D.; Cardiff, R. D.; MacLeod, C. L. Polyomavirus middle T-induced mammary intraepithelial neoplasia outgrowths: single origin, divergent evolution, and multiple outcomes. *Mol. Cancer Ther.* **2004**, *3*, 941−953.
(45) Namba, R.; Young, L. J.; Maglione, J. E.; McGoldrick, E. T.; Liu, S.; Wurz, G. T.; DeGregorio, M. W.; Borowsky, A. D.; MacLeod, C. L.; Cardiff, R. D.; Gregg, J. P. Selective estrogen receptor modulators inhibit growth and progression of premalignant lesions in a mouse model of ductal carcinoma in situ. *Breast Cancer Res.* **2005**, *7*, R881−889.
(46) Namba, R.; Young, L. J.; Abbey, C. K.; Kim, L.; Damonte, P.; Borowsky, A. D.; Qi, J.; Tepper, C. G.; MacLeod, C. L.; Cardiff, R. D.; Gregg, J. P. Rapamycin inhibits growth of premalignant and malignant mammary lesions in a mouse model of ductal carcinoma in situ. *Clin. Cancer Res.* **2006**, *12*, 2613−2621.
(47) Wu, B.; Chien, E. Y. T.; Mol, C. D.; Fenalti, G.; Liu, W.; Katritch, V.; Abagyan, R.; Brooun, A.; Wells, P.; Bi, F. C.; Hamel, D. J.; Kuhn, P.; Handel, T. M.; Cherezov, V.; Stevens, R. C. Structures of the CXCR4 chemokine GPCR with small-molecule and cyclic peptide antagonists. *Science* **2010**, *330*, 1066−1071.
(48) Tanaka, T.; Nomura, W.; Narumi, T.; Masuda, A.; Tamamura, H. Bivalent ligands of CXCR4 with rigid linkers for elucidation of the dimerization state in cells. *J. Am. Chem. Soc.* **2010**, *132*, 15899−15901.
(49) Yim, C. B.; Boerman, O. C.; de Visser, M.; de Jong, M.; Dechesne, A. C.; Rijkers, D. T. S.; Liskamp, R. M. J. Versatile

conjugation of octreotide to dendrimers by cycloaddition ("click") chemistry to yield high-affinity multivalent cyclic peptide dendrimers. *Bioconjugate Chem.* **2009**, *20*, 1323−1331.

(50) Yim, C. B.; Dijkgraaf, I.; Merkx, R.; Versluis, C.; Eek, A.; Mulder, G. E.; Rijkers, D. T. S.; Boerman, O. C.; Liskamp, R. M. J. Synthesis of DOTA-conjugated multimeric [Tyr^3]octreotide peptides via a combination of Cu(I)-catalyzed "click" cycloaddition and thio acid/sulfonyl azide "sulfo-click" amidation and their in vivo evaluation. *J. Med. Chem.* **2010**, *53*, 3944−3953.

(51) Albertazzi, L.; Serresi, M.; Albanese, A.; Beltram, F. Dendrimer internalization and intracellular trafficking in living cells. *Mol. Pharmaceutics* **2010**, *7*, 680−688.

(52) Buckle, T.; van den Berg, N. S.; Kuil, J.; Bunschoten, A.; Oldenburg, J.; Borowsky, A. D..; Wesseling, J.; Masada, R.; Oishi, S.; Fujii, N.; van Leeuwen, F. W. B. Non-invasive longitudinal imaging of tumor progression using an ^{111}indium labeled CXCR4 peptide antagonist. *Am. J. Nucl. Med. Mol. Imaging* **2011**, accepted.